Carbon Blooms & CFCs

Brief summary from published papers. Figure and Table numbers from the original references have not been changed so that the interested reader can quickly look up the relevant sections in the original reference. This document is for NSTX-U internal use only.

R. Raman

13 May 2017

Table of Contents

Carbon blooms

In general, C-bloom starts at 1800C ±150^{0}C on JET vs. 1600^{0}C ±150^{0}C in TFTR.[1]

Misalignments or damage to tiles were the primary location of the C-blooms (hot spots) [Ref. 2]

There is a tile temperature and energy threshold for the carbon bloom.

The radial distance between the hotspot and the last closed flux surface has a strong influence on the temperature threshold. If the hotspot is close to the last closed flux surface, the carbon can more easily get into the plasma.

There were localized areas on TFTR (a few tens of cm^2) on the TFTR RF limiter that reached 3000C bud did not lead to blooms or any increase in carbon influx rate. These areas were about 5cm from the last closed flux surface [Ref 2].

If the radiated power in the plasma is high enough to reduce the power load to the PFC, the carbon bloom can be extinguished. Carbon blooms can appear and disappear.

Methods for avoiding carbon blooms

Change PFC material:
JET switched from CFCs to be tiles to avoid C blooms

TFTR switched from POCO graphite to 4D-CFCs, and tile alignment improved to ±0.5mm accuracy. This allowed the carbon blooms to be increased from starting at 15MJ to 46MJ. The CFC material has higher thermal conductivity (by 20%), higher density (by 10%), and factor of 2 higher thermal shock resistance. This resulted in significantly reduced carbon blooms in TFTR.

Flux Sweeping:
On JET, flux sweeping over a 10cm distance allowed the threshold for blooms to be increased by 10 to 20% (perhaps it can be increased even more by increasing the sweeping frequency which was not mentioned in this paper).

By moving the plasma up and down in a double null configuration the threshold power was increased by 30%.

Good PFC Design:
Apparently DIII-D and JT-60 do not see carbon blooms because of better divertor plate designs?

On JET, switching from fine-grained graphite to CFCs, with improved alignment of the tiles, and increasing the toroidal and poloidal wetted areas allowed operating heat flux to the tiles to be increased.

Similarly, on TFTR switching from POCO graphite to 4D graphite, with improved tile alignment, allowed the divertor heat loads to be increased.

Divertor Gas Puffing:
With divertor gas puffing, JET has operated at 8MW for 6s, vs. 2.5s without gas puffing. However, the increased edge density reduced beam penetration and reduced neutron yield.

Tests in support of graphite materials for ITER

This contains a brief summary from the following report [Ref 6]:
Analysis of Carbon Based Materials (CBSs) under Fusion Relevant Thermal Loads.

This is a over 132 page document with a large amount of information. I have extracted text that I think is of most relevance to the NSTX-U project. The original references to other material in the document are left as in the original document as this allows the interested person to quickly look at the figures and sections not included in this condensed version.

Although nine different versions of graphite were tested, the report does not, in the end, grade them form 1 to 9, with 1 being the best material and 9 the worst.

Acronyms

Brittle Destruction (BD) mechanism
Carbon Based Materials (CBSs)
Carbon Fiber Composites (CFCs)
room temperature (RT)

Why CFCs for ITER?

Thermo-mechanical constraints created during transient heat loads (few GW/m^{2}can be deposited in few ms) are so high that carbon/carbon composites (so-called Carbon Fiber Composites (CFCs)) are better suited than fine grained graphite. CFCs can achieve superior thermal conductivity as well as mechanical properties than fine grain graphite. However, all the thermo-mechanical properties of CFCs are highly dependent on the loading direction as a consequence of the graphite structure.

Nine advanced CBMs (carbon based materials) were compared in terms of microstructure and thermo-mechanical properties. Among them, two fine grain graphites were considered as useful reference materials to allow comparing advantages reached by the developed CFCs.

Thermo-physical properties such as thermal conductivity and thermal expansion of some CFCs were studied for different materials' orientations.

CFCs are long to design and also to produce, in addition large amounts (several tons) are required with constant properties, so no public institutes but private companies are involved in the CFC production. As a consequence of the concurrency between them and the fact that theses materials are considered as strategic nuclear grades; relatively few details about the production are disclosed leading to some gaps in the material's production history.

Structure of graphite

Carbon has a unique property of being able to form bonds between its atom creating stable compounds such as chains, branched chains and rings. Carbon has a number of distinct molecular or crystalline forms termed allotropes, which include graphite, diamond and fullerenes. This gives to carbon extreme variations in physical properties.

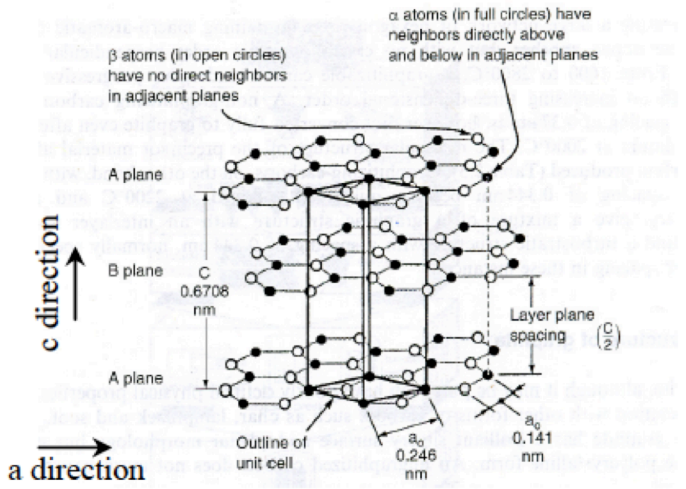

Fig. 9 : Hexagonal unit cell structure of graphite [50]

Graphite is defined as an allotropic form of the element carbon consisting of layers of hexagonally arranged carbon atoms in a planar condensed ring system with each carbon 0.141 nm from its three nearest neighbors (Fig. 9).

The layers, termed graphene layers, are stacked parallel to each other in a three dimensional structure. The chemical bonds within the layers, between each carbon atom, are covalent (**σ**); each hexagonal array forming six **σ** bonds (of high strength: 524 kJ.mol-1) and the remaining p orbitals, which are at right angles to the graphene layers, take no part in the **σ** hybridization. The p orbitals of two neighboring carbon atoms overlap sideways and form **π** orbitals, with three above and three below the **σ** orbital plane. The **π** orbitals in each hexagonal array overlap and encircle all six carbon atoms taking up the form of a torus and the six electrons become delocalized throughout the **π** orbital, which lowers the energy and helps to stabilize the molecule (aromaticity). The graphene planes are ≈ 0.335 nm apart and are held only with weak forces (7 kJ.mol-1), which are comparable with van der Waals forces.

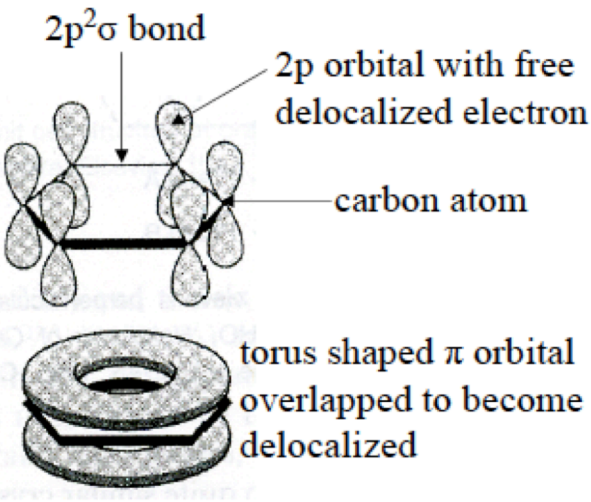

Fig. 10: The p-orbitals

As an illustration the theoretical Young's modulus in the grapheme

plane (a direction) is 1050 GPa whereas in the c direction it is 35 GPa; thermal and electrical conductivities in the c direction are lower by two orders of magnitude than those in the a directions. Such anisotropy in the crystal underlies the behavior in bulk and has relevance to the fiber and matrix constituents of CFCs (see chapter 2.3.1. and 2.3.3.), but there are other factors to be considered such as the angular dependence of the thermal (see chapter 3.1.2.) and mechanical (see chapter 3.2.1) responses.

CFCs

CFCs are constituted of carbon fibers of various lengths and placed at various orientations, depending on the planned application, to obtain a so-called preform within which a carbon matrix is infiltrated to densify it.

Globally, the carbon fibers properties are anisotropic and reflect the degree of orientation of the graphene layers within the fibers.

The investigated CBMs in this work are listed in Table 3. Among those are two fine grain graphites and seven CFCs. CX2002U is the Japanese reference material for the outer divertor of ITER, and NB31, NB41, 3D-DUNLOP and DMS780 are considered for the inner divertor of ITER. For practical purpose, CFCs are subdivided in three groups called in this work: 3D, 2D and felt types as described in Table 3.

material	manufacturer	fine grain graphite	CFC type
R6650	SGL	X	-
AXF-5Q	POCO	X	-
NB31	SNECMA		3D
NB41	SNECMA		3D
3D-DUNLOP	DUNLOP		3D
DMS704	DUNLOP		2D
DMS780	DUNLOP		2D
CX2002U	TOYO TANSO		felt
AO35	CARBONE LORRAINE		felt

Table 3 : List of the investigated CBMs

The fine grain graphites are the materials which were used in the past decades in the fusion devices or in the devices of rather small sizes. For facilities of the size of ITER, the mechanical properties of fine grain graphite are insufficient to sustain the thermomechanical loads created by the energetic plasma particles as well as the magnetic fields owing through the PFMs. Nevertheless, in this comparative study, it is very useful to refer to the fine grain graphites as basic materials.

For the description of CFCs, it is essential to explain the nomenclature used within the

fusion community for their three orthotropic directions. The X direction is the direction with the highest thermal conductivity, Y the one with intermediate thermal conductivity and Z the one with the lowest [10]. The relative thermal conductivity is related to the material type and content aligned in each respective direction. On the contrary, the used graphites are considered as macroscopically isotropic in terms of thermo-mechanical properties.

NB31 (all batches), NB41 [83] and 3D-DUNLOP (called "new DUNLOP" in [84]) are unbalanced cross-ply laminates (0°/90°) reinforced by a needling process in the third orthogonal direction (Z) [64].

In comparison to the previously described CFCs, CX2002U and AO35 are of so-called felt type. They are not constituted of groups of thousands of long fibers oriented in different directions but smaller groups of short fibers which are preferentially aligned and punched by needles in various directions. AO35 is made of PAN fibers while CX2002U is made of rayon fibers.

For fusion application, the most important is the X direction and blocks are usually limited to a thickness below 10 cm in this direction. This thickness is nonetheless considered as very challenging.

Density of Graphite

Crystallographically perfect graphite has a density of 2.265 g.cm-3. The density of synthetic graphite is rarely above 2.0 g.cm-3, and is directly related to the porosity. Decreasing the particle size, or grain, does in general lead to reduce the relative porosity. Manufactured carbons contain many types of imperfection when compared to the graphite crystal. Prominent among these are voids, which may range in size from single atom vacancies within the crystal up to large pores in the disordered regions between crystallites. Density is a particularly important parameter in describing carbons of all types as it gives an insight into the degree of crystalline perfection as well as governing many of their physical properties (see chapter 3.1.2.).

The average densities, provided by the manufacturers, of all studied CBMs are reported in Table 6. It is interesting to note that the density of R6650 is slightly lower than the one of AXF-5Q, and this, even if the observed porosity (see Fig. 27) seemed to lead to the opposite conclusion. This means that constituents of AXF-5Q have higher individual densities. Consequently the average density cannot directly be related to the material porosity. Wide ranges of densities can be obtained depending on the carbon precursor; however they are all lower than the theoretical density of graphite crystal if no heavier impurity than carbon is present.

material	average density [g.cm^{-3}]
R6650	1.85
AXF-5Q	1.86
NB31	1.87
NB41	1.94
3D-DUNLOP	1.83
DMS704	1.87
DMS780	1.81
CX2002U	1.67
AO35	1.78

Table 6 : Average densities of the studied CBMs (manufacturers' data).

The density of felt materials is in general, and here in particular, much lower than the ones of laminate CFCs. The fact that the felt preforms are very porous structures and the aim of achieving high thermal conductivity materials can be in contradiction. The presence of porosities has a negative impact on the thermal conductivity since air is considered as thermal isolator in comparison with graphitic structures (even in the c direction). This could indicate that fully densified materials are theoretically the best heat conductor. However densification should not be performed at the expense of the degree of orientation of the matrix, homogeneous and highly oriented matrix has to prevail over more isotropic matrix.

Thermal conductivity of graphite

For the determination of the thermal conductivity of the various CFCs and in order to fully characterize their anisotropy, different orientations were investigated and are presented in Fig. 45. The X, Y, Z are the standard orientations while the tilted ones (15°, 30° and 45°) where especially produced to understand the off-axis thermo-physical response of CFCs and to generate a reliable and more complete database which might be used for modeling purpose.

In Table 7, the RT thermal conductivity values of all the investigated CBMs are displayed for various orientations. These data should be regarded as indications and not fixed values since large discrepancies can be found during tests and within literature, though they allow drawing conclusions. The thermal conductivity anisotropy of CFCs is clearly visible and must be related to the fiber architecture. DMS704 and DMS780 have equivalent thermal conductivity in their X and Y directions due to their balanced architecture and the use of the same carbon fibers in both directions. The thermal conductivity of felt materials is very different between CX2002U and AO35 with a clear advantage for the first. This can be due to the presence of a more homogeneously deposited matrix for CX2002U, which is believed to play the main role in thermal transport in CFCs as the major constituent in terms of vol. %. Thermal conductivity

values of CX2002U exceeds the best investigated 3D or 2D CFCs even if it is a very porous material, meaning that the constituents are from higher quality and/or that the fiber architecture favors thermal transport.

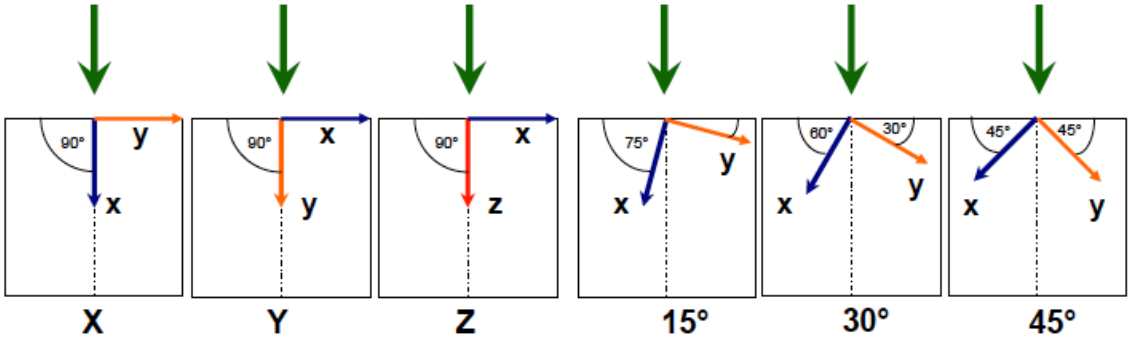

Fig. 45 : Sketch of the used orientations in this work, the green arrows symbolize the thermal or mechanical load direction

Fig. 46 is a good example to show how the thermal conductivity is highly anisotropic in CFCs, decreases for increasing temperatures and may be influenced by density.

	RT thermal conductivity [$W.m^{-1}.K^{-1}$] in direction		
material	X	Y	Z
R6650	90	-	-
AXF-5Q	90	-	-
NB31	320	120	90
NB41	400	110	70
3D-DUNLOP	300	120	50
DMS704	300	300	70
DMS780	300	300	70
CX2002U	410	310	170
AO35	100	100	75

Table 7 : Average RT thermal conductivity of the investigated CBMs.

Fig. 48 gives evidence that the difference of thermal conductivity in between the tilted orientations (15°, 30° and 45°) can be rather high at room temperature while becoming negligible at high temperatures (see also annex 4).

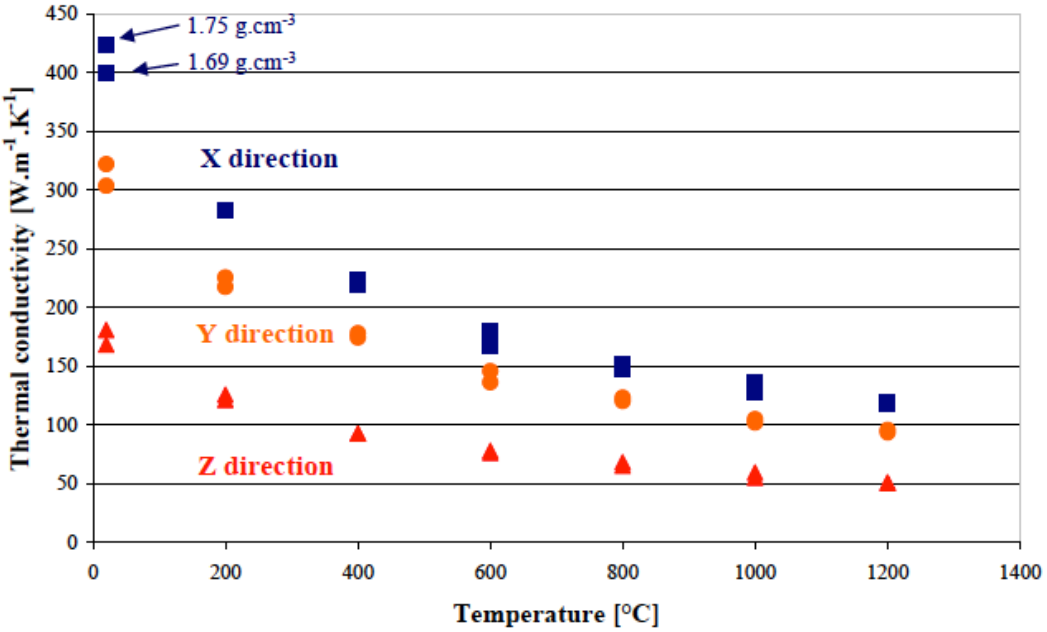

Fig. 46 : Example of thermal conductivity in the X, Y, Z directions of CX2002U as a function of temperature

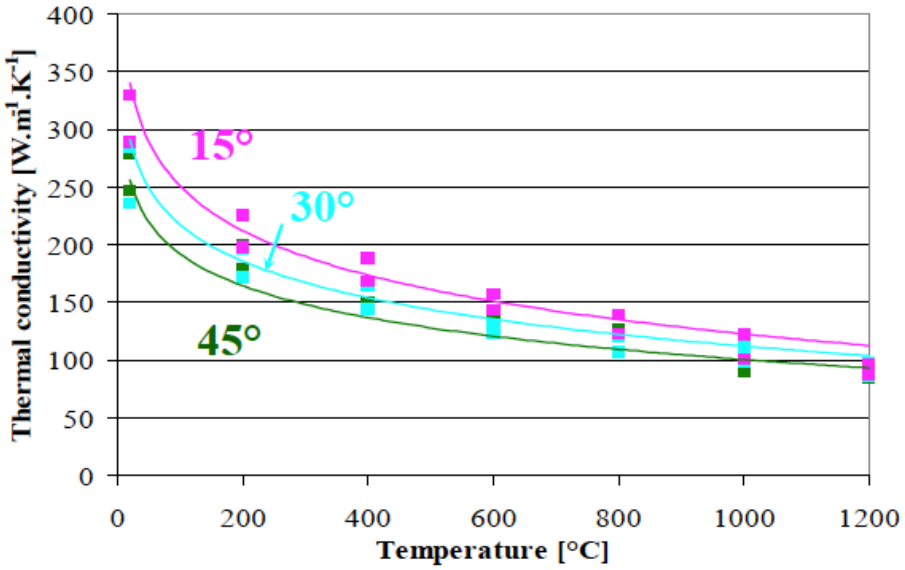

Fig. 48 : Thermal conductivity of DMS780 for the tilted orientations (15°, 30° and 45°) as a function of temperature.

It is known that the transverse conductivity of individual fibers can be as low as 100 times less the one in the longitudinal direction but in a laminate with the presence of a highly oriented matrix between the adjacent constituents, the transverse conductivity can reach values only four times lower than in the longitudinal direction [100]. The heat conduction path trough laminates, via connected layer planes of matrix around adjacent fibers, has been depicted in [97,100]. This explains why RT thermal conductivities above 50 W.m-1.K-1 are observed in the studied CFCs while only a very small vol. % of fibers is aligned in this direction.

Thermal expansion of graphite

The graphite crystal is also highly anisotropic concerning its thermal expansion. Graphite expands in the c direction while it contracts in the a direction up to about 400°C [104]. As a consequence all the graphitic structures will have anisotropic thermal expansion too.

Results for CX2002U are plotted in Fig. 49, they clearly demonstrate that the thermal expansion in the Z direction is significantly higher than in the X and Y direction. The thermal expansion in the Z direction of CFCs is usually the highest of the three main directions (X, Y, Z) since it provides the largest amount of transversally oriented fibers.

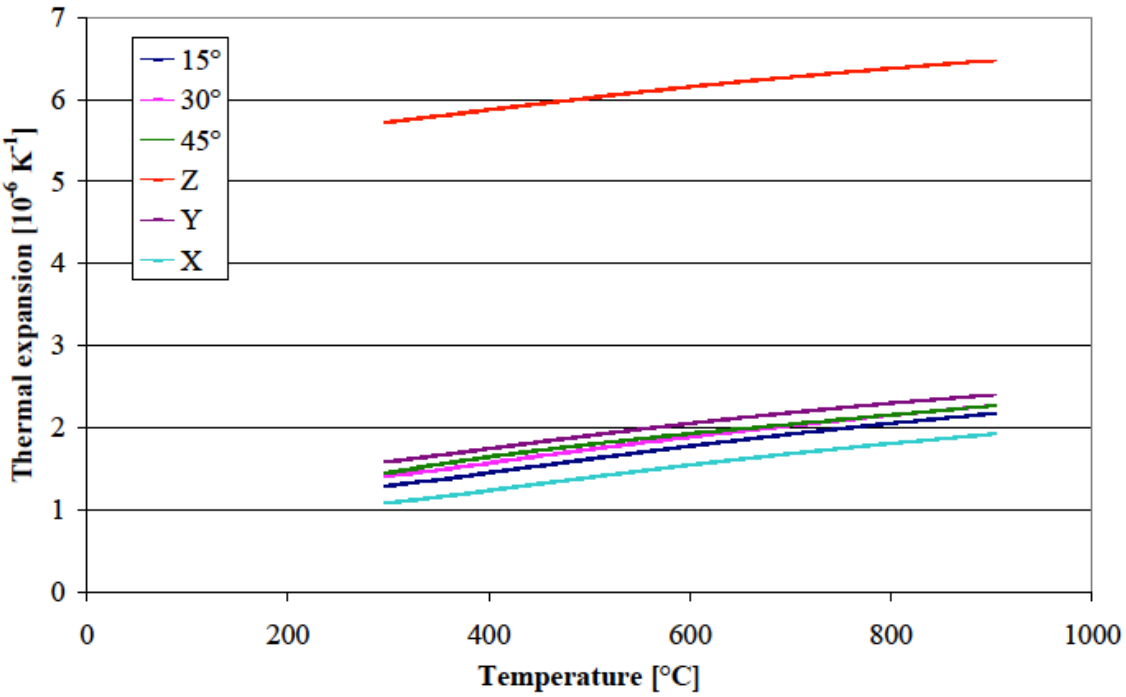

Fig. 49 : Thermal expansion of various orientations of CX2002U as a function of temperature.

Mechanical strength of graphite

Despite attractive properties (chapter 1.7.), fine grain graphite suffers from two serious drawbacks which are its mechanical weakness and its brittle type of failure.

Like for graphite, the strength of CFCs increases at elevated temperatures, reaching a maximum at about 1500 °C. This can be explained by the fact that during cooling-down from the production temperature of CBMs to RT, micro-cracks or even pores have been preferentially formed between the various constituents. Their formation leads to internal stresses/strains around and at their interfaces. When mechanical tests are performed at high temperatures, the materials expand and tend to fill the pores and cracks (phenomenon called crack bridging). It reduces the number of sites, which were acting as crack initiator and internal stresses/strains. Above 1500°C there is a continuous decrease such that at 2000 °C the strength is substantially the same as at room temperature and above 2000 °C plasticity becomes apparent characterized by the fall in Young's modulus and the rise in strain.

A compilation of tensile strength and Young's moduli of most of the investigated CBMs is displayed in Table 8. CFCs of the type 2D and 3D reach values much superior to fine grain graphite in some of their directions while felt type CFCs (CX2002U and AO35) never exceed them. NB41 (X) has the highest mechanical properties of all the studied CBMs in their respective strongest direction. The 3D CFCs have the highest anisotropy in terms of mechanical properties while felt CFCs have the lowest one among composites. The studied fine grain graphites have isotropic properties exceeding the ones of the investigated felt CFCs.

	RT tensile strength [MPa] in direction			RT Young's modulus [GPa] in direction		
material	X	Y	Z	X	Y	Z
R6650	50	-	-	12.5	-	-
AXF-5Q	62	-	-	11	-	-
NB31 (pilot)	130	30	19	107	15	12
NB41	220	40	12	188	22	9
3D-DUNLOP	101	55	9	83	21	8
DMS780	110	110	15	55	55	6
CX2002U	35	31	11	10.7	8.1	3.4
AO35	40	≤ 40	≤ 40	11	≤ 11	≤ 11

Table 8 : RT tensile strength and Young's moduli of most the investigated CBMs. Data from NB31, NB41 and 3D-DUNLOP were measured over large number of specimens [88, 89]. The other data are from the manufacturers.

NB41 has the highest mechanical properties of all the investigated CBMs, irrespectively of the considered direction.

Thermal Shock Testing

The energy deposited on PFMs during transient events is very high in terms of power density (few $GW.m^{-2}$) and their duration is very short time (few ms or less). This will

create tremendous thermo-mechanical stresses in the top surface of PFMs leading to thermal erosion in various forms.

Thermal shock experiments have been performed on CBMs in the past [129-134] but only few of them are directly comparable due to the different types of impinging particles (electrons, various ions, photons), power densities and pulse durations which were used. Nonetheless, a widely accepted heat flux parameter F, described in Equation 5, is used in the community to compare various facilities in terms of deposited heat. F concretely indicates the heat flux which is consumed for the increase of the surface temperature of the heat loaded sample [133] so that the influence of the type of particle can be neglected. This factor is suited for the simulation of one-dimensional heat conduction under short pulse thermal loads.

$$\text{Equation 5 : } F = \frac{P}{A} \times \sqrt{t}$$

Where P stands for the absorbed power [MW], A for the loaded area [m^2] and t for the duration [s] of the heat flux. ELM load in ITER are predicted to be of 0.5 to 1.5 $MJ.m^{-2}$ for a duration of 500 **µ**s, which corresponds to heat flux parameter of 22.4 to 67.1 $MW.m^{-2}$.s1/2.

Heat flux texting facility

Most of the thermal shock load experiments presented was performed in the electron beam facility JUDITH (Forschungszentrum Juelich, Germany) (Fig. 66). JUDITH has a maximum power of 60kW and generates electrons with energies of 120 keV. Electrons of such an energy penetrate about 70 **µ**m within the bulk of CBMs (volumetric heating) but do not initiate lattice defects [137]. The beam has a diameter of about 1 mm and scanning of the beam is realized in the X-Y plane at frequencies around 50 kHz in order to obtain a homogeneous thermal loading. The beam is impinging perpendicularly to the sample surface. The samples are loaded in vacuum (about 10^{-3} Pa). The pulse duration can be from 1 ms to continuous (for steady state loading tests), reflecting the flexibility of the electron-beam facilities. The deposited power density (CBMs absorb about 90% of the incident electrons at 120 keV) was up to 10 GW.m-2 (F≈ 316 $MW.m^{-2}$.s1/2) in the performed experiment.

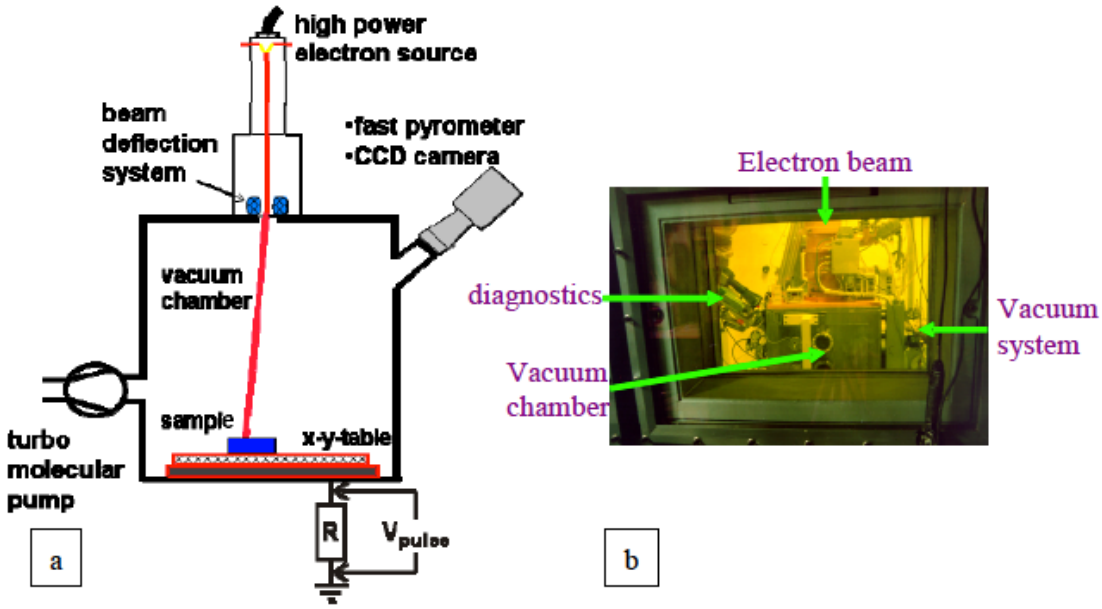

Fig. 66 : a) Sketch of thermal shock loading within JUDITH, b) Optical picture of JUDITH installed in the hot cells of Forschungszentrum Juelich.

Thermal erosion

CBMs do not melt under fusion relevant thermal shock loads, which is one of their main advantages. However, they do sublimate when temperature above approximately 3000°C are achieved. For graphites, the binder phase has a less ordered structure than the grain so its thermal conductivity is lower and it will thus more easily reach the sublimation temperature. This will lead to preferential erosion of the binder phase.

Brittle Destruction

The ejection of hot particles from the surface of CBMs under thermal shock loads, so called brittle destruction (BD) has been investigated [27,130,140,141]. BD is due to the presence of constituents within fine grain graphite or CFCs, with different thermal expansion and thermal conductivity. The fact that some constituents overheat due to their lower thermal conductivity will create local stresses at the various interfaces.

When power densities used were higher (usually above 1.6 GW.m-2 (for CFCs) for a pulse duration of 5 ms), brittle destruction (BD) occurred, i.e. emission of hot particles or intersected fibers from the material's surface.

This has been explained by differences of thermal conductivity and thermal expansion of the constituents at various scales leading to tremendous tensile stresses at their interface. These stresses can be released by BD processes during and still shortly after disruption loads.

Weight Loss

Weight loss results of all the CBMs after a single 5 ms fusion-relevant disruption in JUDITH are plotted in Fig. 85 (CFCs were loaded in their X direction). As shown in Fig. 85, the CBMs were classified into three groups: the fine grain graphites and AO35 with the highest weight loss, DMS704 and DMS780 with intermediate weight loss and NB31, NB41, 3D-DUNLOP and CX2002U. No weight loss was detectable for single disruption with a power density lower than 1.6 GW.m^{-2}. This criterion is a useful basis for comparison of thermal shock resistance between CBMs. The interest of this plotting is that we could theoretically extrapolate the values at which no weight loss will be observed for a 5 ms disruption load. Another important aspect is that weight loss is mostly related to the RT thermal conductivity of the CBMs and not to the mechanical properties (see table 8) since AO35 belongs to the group with the highest erosion rate while CX2002U to the one with the lowest. Nevertheless, to better describe the thermal shock resistance of CBMs and to be able to compare them, their density should be taken into account since this will define the eroded thickness, if the erosion pattern would be homogeneous! It is in fact not the case as it will be described in more details hereafter. Another important observation is that the higher will be the absorbed power density, the higher will be the influence of BD on the overall weight loss since the generated thermal stresses will ramp-up at a faster speed.

It was observed that weight loss during thermal shock loads is a combination of both thermal erosion and BD, in ratios which are yet hardly quantifiable and a function of the type of CBM. However, thanks to precise experimental methodology used during simulated plasma disruptions load in the electron beam JUDITH, an experimental thermal shock resistance criterion could be established. It relies on the weight loss per surface area, which occurs under various thermal loading conditions. 3D CFCs and CX2002U exhibit the lowest weight losses while the two isotropic fine grain graphites and AO35 have area-related weight losses up to four times higher.

It was observed that the disruption loads on fine grain graphites and on CFCs do not lead to the same types of erosion processes. For the fine grain graphite AXF-5Q, a strong light emission from the surface (which might be associated with the presence of carbon vapor cloud) and very small tracks of hot particles can be seen, whereas for CFCs, a lower light emission above the target is observed but larger linear tracks are visible. Much clearer tracks (larger and/or hotter particles) can be seen for DM780 and NB31 than for CX2002U. This is probably due to the fact that rather large groups of fibers are ejected from the two first CFCs as only individual fibers are ejected from CX2002U as a consequence of their respective fiber architectures. The presence of a strong light emission above the surface of AXF-5Q most likely implies that sublimation takes a large place in the weight loss of this material while erosion for CFCs seems to be largely dominated by BD. It was demonstrated that the proportion and size of tracks are correlated to the material microstructure and to the size of the constituents of the CBMs.

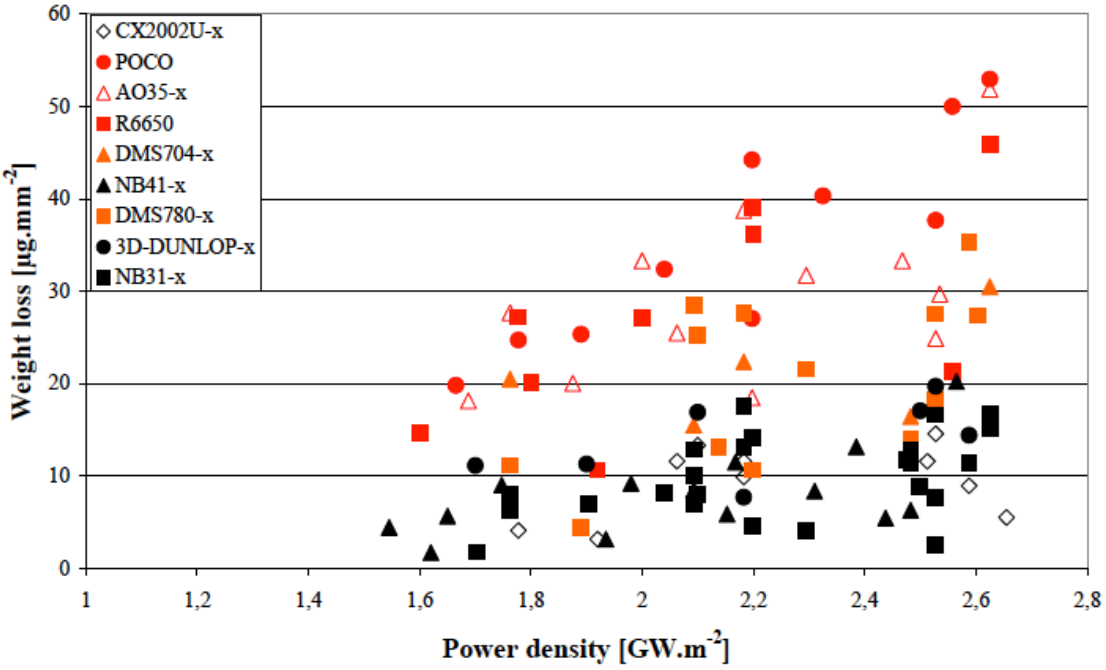

Fig. 88 : weight loss per area for all the studied CBMs under single disruptions loads of 5 ms performed in JUDITH

Since BD in laminate CFC was theoretically explained and supported by finite element methods, attempts to reduce it by appropriate material off-axis tilting (between X and Y directions) were undertaken. It was successful in many cases for single transient loads. This success was attributed to the lower temperature differences between the tilted X and Y laminates leading to lower thermal stresses while providing a better mechanical attachment of the Y laminate to the bulk. However when repeated simulated plasma disruptions were applied, i.e. BD contribution to material erosion is reduced in relation to sublimation, the lower macroscopic thermal conductivity of the tilted CFCs was the most influencing factor and weight loss of tilted materials increased with the tilting angle. Very atypical eroded surface profiles were observed in these experiments. Similar erosion 94 patterns might be obtained in fusion devices if penetrating species would impinge at various angles on the CFC surfaces.

Thermal shock tests on CFCs under various orientations

BD of CFCs is related to the anisotropic properties of the constituents as well as their orientations in regards to the heat flux. For the CFCs described in this work as 3D, it is known that the thermal conductivity of the X direction is higher that the one of the Y direction (see table 7), irrespectively of the vol. %, this due to the different fibers used. Thermal shock loading of these CFCs in the Y direction should allow verifying if lying the fibers with the highest thermal conductivity parallel to the surface could effectively remove the heat from the loaded area resulting in a lower temperature difference between two adjacent laminates. In addition the fibers in the X laminates have higher mechanical properties and should thus be more resistant to thermal stresses. Unfortunately, it was

observed that the pitch fibers were largely broken and pulled out from the disruption loaded surface (Fig. 95). Fig. 95b brings additional evidence that matrix is primarily eroded when aligned perpendicularly to the surface, as a consequence of its weak mechanical properties leading to premature loss of contact and further ability to diffuse the heat within the bulk, as explained in chapter 3.3.2.

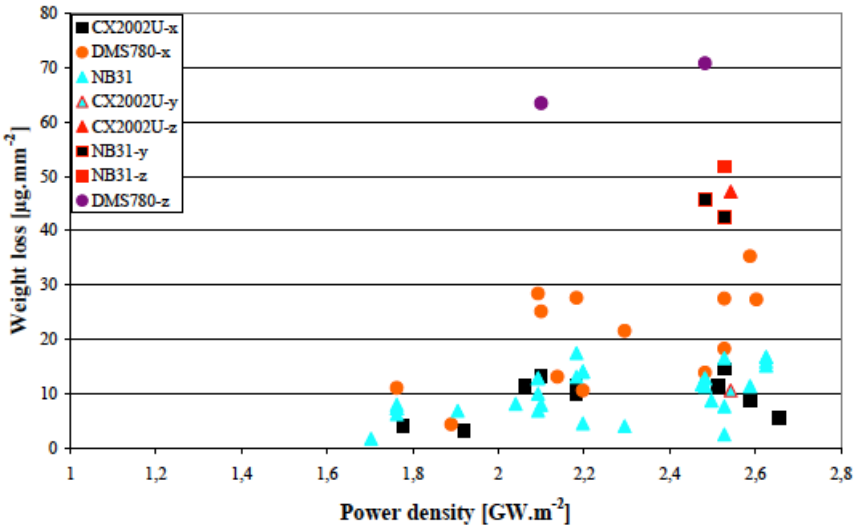

Fig. 97 : weight loss of NB31, DMS780 and CX2002U in X,Y, Z orientations under single disruption of 5 ms in JUDITH

Disruption loads were applied on CFCs in their Z direction where very few short fibers (needling fibers) are facing the heat flux. This conducted to large fibers erosion and ejection but also to deep and rather homogeneous craters for the Z directions while a large preferential erosion-ejection of X laminates was observed for the Y samples (Fig. 96 and [143]). In both cases, these large erosions are correlated with high weight losses (Fig. 97).

It is understood that the difference of temperature between two orthogonal and adjacent laminates is the prime reason why BD occurs. Thus thermal shock specimens were produced at tilted orientations (15°, 30° and 45° as described in Fig. 45). As the angular evolution of thermal conductivity within laminates was described in Equation 3 and macroscopic thermal conductivity of the tilted orientations were measured to confirm it (chapter 3.1.2.), success in limiting BD was thus expected. In addition, tilted Y laminates have higher mechanical attachment compared to Y laminates lying parallel to the surface plane [144], so delamination and ejection from fibers of the tilted Y laminates should be more difficult to be realized.

During thermal shock loads, the macroscopic surface temperature could be measured by means of a fast pyrometer [138] (Temperature range/ 500-2500°C). As it was expected from the macroscopic thermal conductivity of the different investigated directions, the Z

direction is the one reaching 2500°C the fastest (the maximum temperature for the used pyrometer), then comes the sample in the Y direction.
The sample which achieved the lowest temperatures is the one loaded along the X direction. The tilted materials display intermediate surface temperature included in between the ones of the X and Y directions and increasing with the tilting angle (Fig. 98).

Even if the macroscopic surface temperatures of the tilted CFCs are higher than the samples oriented in X direction, lower weight losses were measured on many of them after single disruption (Fig. 99 and Annex 9).

When the surface profiles of these CFCs were analyzed after single disruption loads one observed that preferential erosion is significantly reduced for samples with the most inclined Y laminates or direction. In the case of the 45° samples, neither strong erosion of the Y laminates was observed nor pulled-out fibers (Fig. 100). It seemed to be very successful in limiting BD (see [143]).

When repeated disruptions were done on tilted materials an increase of weight loss in comparison to the X direction was observed as the tilting angle was larger (Fig. 101). The weight loss values of the various tested CFCs was about twice higher in the 45° titled sample compared to the X direction. The fact that the weight loss values were smaller than the ones after a single disruption, confirms once again that the weight loss per shot (for the number of disruptions investigated herein) is maximal during the first shots.

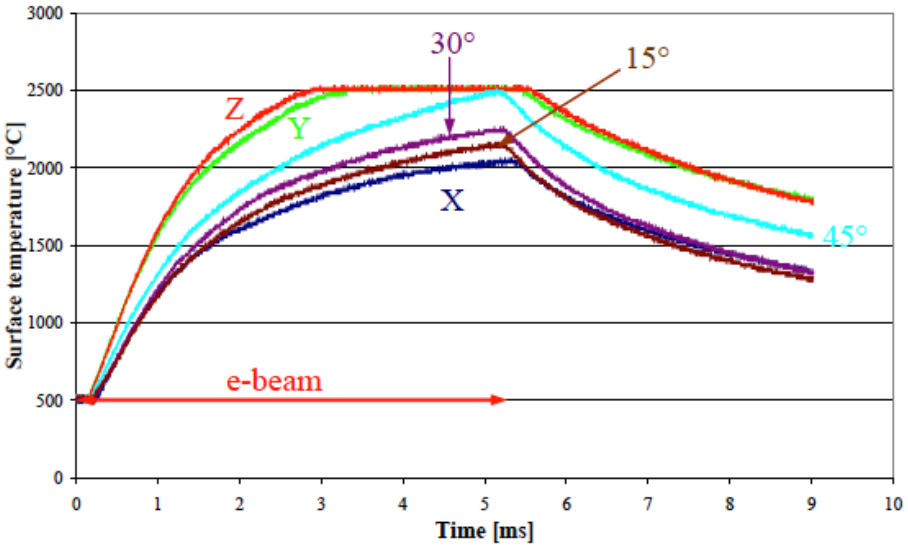

Fig. 98 : surface temperature of NB31 loaded under various orientations with JUDITH (single disruption of about 2.5 GW.m^{-2} and 5 ms)

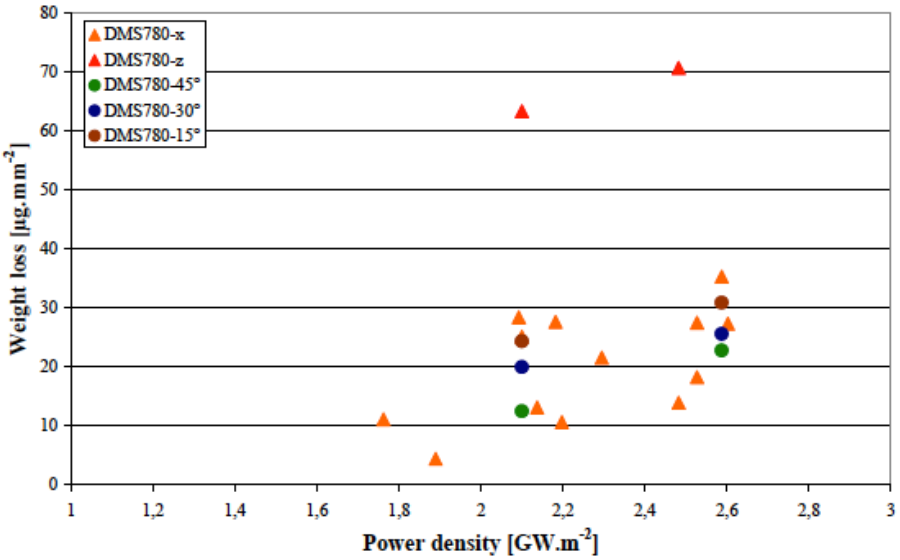

Fig. 99 : weight loss of DMS780 in various orientations after single disruptions of 5 ms in JUDITH

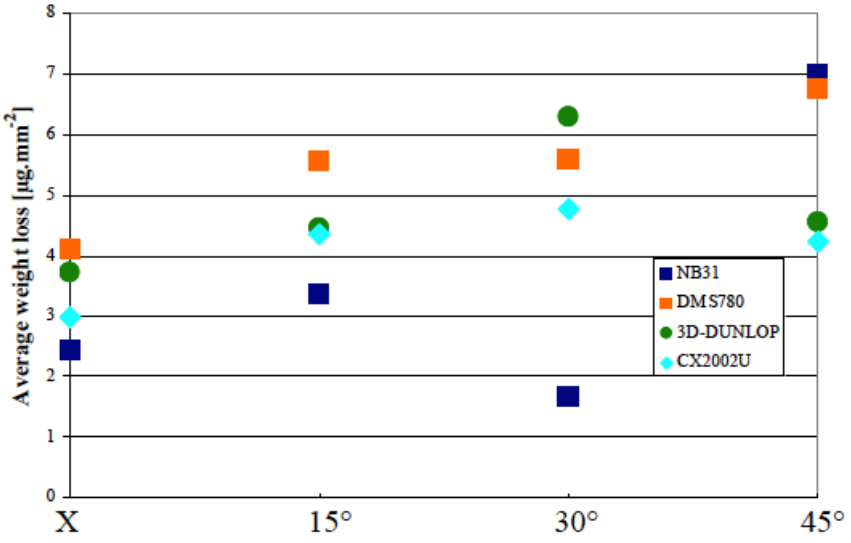

Fig. 101 : Average weight loss for various CFCs under different orientations after nine disruption loads of about 2.5 GW.m^{-2} and 5 ms on previously loaded positions

The surface profiles confirmed that the craters created on tilted samples after repeated shots were clearly deeper and larger in the case of the 45° direction compared to the X direction (Fig. 102). This figure highlights the fact that the felt layers of DMS780 are preferentially eroded compared to the laminates, confirming their lower thermal conductivity. Surface profiles of DMS780, NB31, CX2002U and 3D-DUNLOP after 5 and 10 disruptions under various material orientations as well as SEM micrographs of the centre of the loaded areas after 10 disruptions are displayed in Annex 10. As the tilting

angle increases from 0° (X) to 45°, the erosion of the Y laminates or fibers in the Y direction decreases but the erosion of X laminates starts. For the 45° samples, for most of the CFCs, the thermal erosion is almost the same for the laminates or fibers aligned in the X and Y directions (Fig. 103). No pulled-out fibers were observed and the erosion seems to be dominated by sublimation due to higher surface temperature

JET divertor design

JET Tested Fine grained graphite, CFCs and Be[2]

The Mark II divertor uses CFC tiles (approximately: 40cm x 18cm x 4cm). These can also be made out of Be. See Figure 1 below.

This design has resulted in a calculated maximum power density of <5 MW/m^2 on the tiles for most plasma configurations and up to 15 MW/m^2 for particular discharges (at the full power of 40 MW) out of which 50% is conducted to the tiles.

The toroidal wetted length is optimized by using target tiles, which are long in the toroidal direction and mounted in a way to reduce misalignment. The tiles are attached to tile carrier by a single spring loaded central bolt attached to a dumbbell shaped rod inserted in a hole drilled into the tile, and supported on four corner pads [Ref 1, Fig. 2].

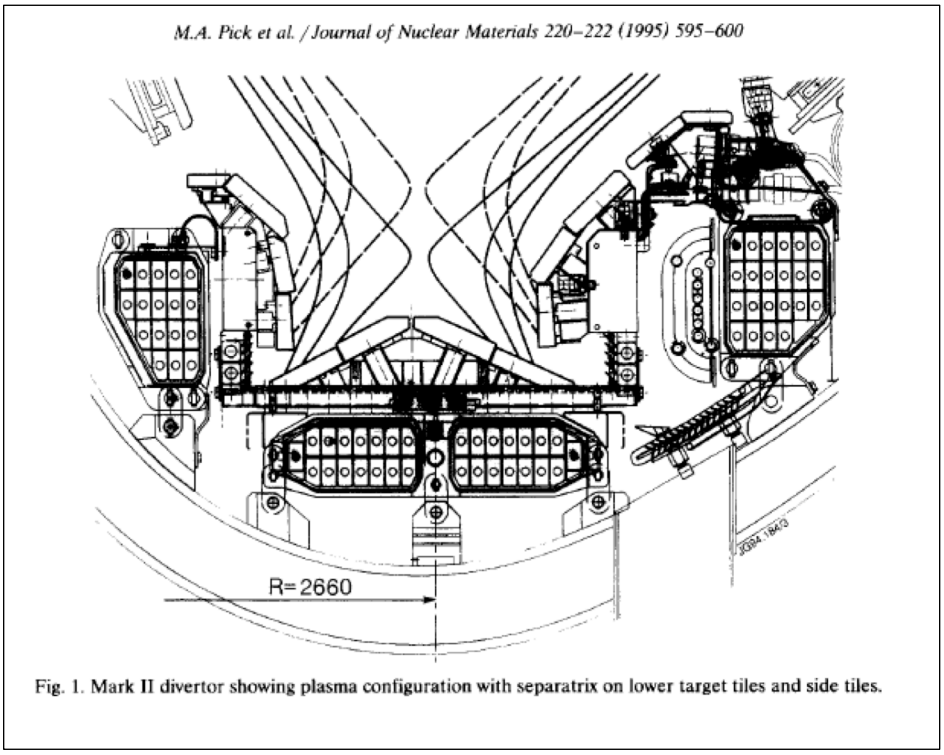

Fig. 1. Mark II divertor showing plasma configuration with separatrix on lower target tiles and side tiles.

The poloidal inclination of the target tiles was chosen so that the poloidal area wetted by the plasma scrape-off is increased as far as possible for the plasma configuratio ns envisaged.

The front surfaces of the tiles do not have holes or cut-outs either for tile attachments or for diagnostic purposes.

Thermal conductivity into tile & low thermal expansion coefficient are important to avoid tile cracking due to thermal heating.

Maximum design limit was 1600^{0}C for all parts of the tiles.

JET divertor tile testing program

JET undertook an extensive testing program.

Firms provided 15cm x 20cm tiles for testing.

These were tested in the JET NBI test bed in the heat flux range of 5 to 30 MW/m^2. Testing concentrated on the thermal conductivity, bowing and mechanical integrity of the tiles.

The time taken for the material to reach 1600^{0}C was regarded as the first figure of merit for the materials. Tests were conducted at 5, 10 and 15 MW/m^2. The results are shown in Table 1 (below). The T02 material takes 11.81 seconds to reach 1600C at 5MW/m^2. The T06 does better, but it is a 1D tile. See the pasted figure in a following page for 1d, 2d and 3d tile configurations.

Table 1
Overview of results of high heat flux tests on Mark II tiles

Test	Material name	Type	Density (g/cm^3)	250–1500°C at 5 MW/m^2(s)	250–1500°C at 10 MW/m^2(s)	300–1500°C at 15 MW/m^2(s)
T02	DMS 704	2D	1.79	11.81	2.84	1.19
T03	DMS 704	2D	1.85	12.94	4.22	1.49
T06	DMS 704 Alt2	~ 1D	1.89	15.84	5.14	1.91
T08	DMS 705P	~ 1D needled	1.73	7.79	1.98	0.86
T12	N11	~ 3D	1.82	9.83	2.44	0.99
T14	1002ZV22	2D	1.53	7.72	1.85	0.86
T15	1502ZV	2D	1.76	7.85	2.44	1.19
T16	1502ZV22	2D	1.73	10.30	2.54	0.99
T17	AO35	~ 3D	1.76	6.86	1.55	0.73
T18	MFC-1	1D	1.97	–	7.5	–

Table 1: DMS704 / T02 tiles were adopted based on cost and test results.

Large size tile bowing and thermal induced cracking

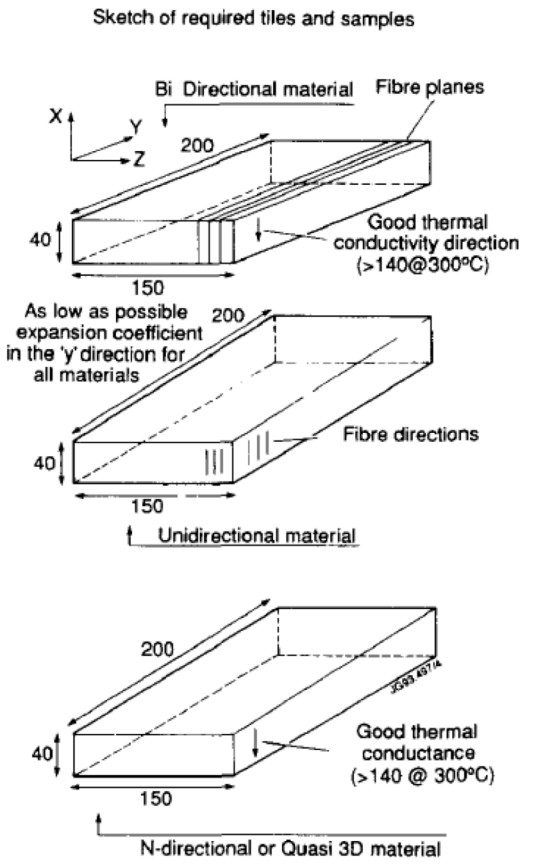

Fig. 3. Required tile material for Mark II divertor.

1D, 2D and 3D Tiles

Bowing up to 1mm was observed in the test tiles.

Because of the large size of the tiles, some tiles tended to crack along the fiber planes. Such cracking had previously not been seen for smaller tiles.

2D materials all cracked after one or a few pulses at ~20 MW/m^2. The quasi 3D or random materials performed well up to the maximum flux density.

As a result of these failures, tests were performed on tiles that were mechanically constrained against cracking as shown below.

The testing showed that in general most of the materials have properties within the limits specified by the manufacturers.

JET tile support structure

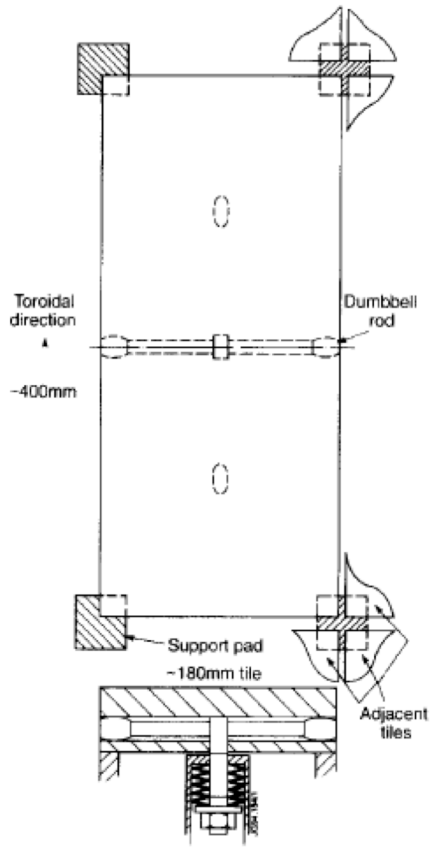

Fig. 2. Target tile support system and attachment system.

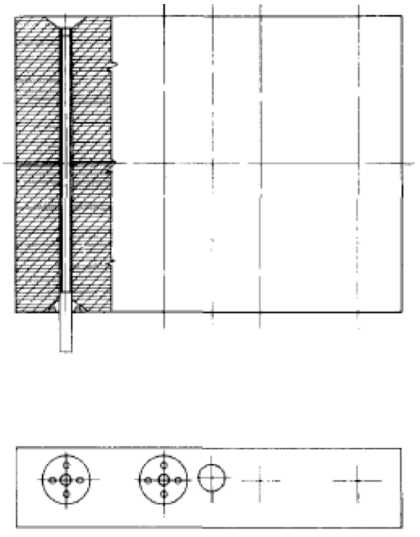

Fig. 4. CFC tile showing inconel 718 tie bars designed to mechanically constrain tile against cracking.

Fig. 2 and 4: JET Tile support structure

Tests were performed on tiles that were mechanically constrained against cracking by the insertion of Inconel 718 tie bars [Ref. 1, Fig. 4, also shown here]. Such tiles performed well with no degradation at 200 pulses at 15 MW/m^2.

The tiles are attached to the tile carrier by a single spring loaded central bolt attached to a dumbbell shaped rod inserted in a hole drilled into the tile, and supported on four corner pads, as shown in the figure 2 on the left.

Note that these tiles may be large compared to the ones planned for NSTX-U. So, thermal cracking may be less of an issue on NSTX-U.

Brief summaries from other papers

Studies for TPX

P.G. Valentine, et al., GA-A22206[3]

High heat flux testing of CFCs conducted using a 30 kW electron beam test system (EBTS) at Sandia & with the Plasma Disruption Simulator (PLADIS-I). 49 different CFC materials tested. See the table below for the list of materials.

Table 1

Summary of the 49 CFC Materials Tested in the EBTS and PLADIS-I Facilities. The test specimen thermal conductivities (k_z) in the direction parallel to the e-beam or plasma-beam are listed at right. F = fiber reinforcement type [proprietary, rayon, PAN, pitch, or vapor-grown carbon fiber (VGCF)]. M = matrix type [none, proprietary, resin, CVI, or pitch].

Manufacturer	Description	Architecture	k_z (at 20°C)
Aerotherm Corporation	HiCond; F = Pitch, M = Pitch	2D	300
	SSN; F = PAN, M = Pitch	3D	220
Alliant Techsystems Inc. (Hercules Aerospace Co.)	ATI 1D; F = Pitch, M = Unknown	1D	Unknown
	HA-PAN 334; F = PAN, M = Pitch	3D	103
	(a) HA-K334; F = Pitch, M = Pitch	3D	170 or 270
	(b) HA-K334; F = Pitch, M = Pitch	3D	270
AlliedSignal Inc.	865-19-4; F = Pitch, M = CVI	3D	221
Amoco Performance Products, Inc.	(a) ThermalGraph 8000 Panel; F = Pitch, M = None	1D	25
	(b) ThermalGraph 8000 Panel; F = Pitch, M = None	1D	750
Applied Sciences, Inc.	ASI 1D; F = VGCF, M = CVI+Pitch	1D	900
BF Goodrich Aerospace	BFG 1D; F = Pitch, M = CVI+Pitch	1D	650
	(a) C-251 Hi-K Unbalanced Weave; F = PAN, M = CVI	2D	89
	(b) C-251 Hi-K Unbalanced Weave; F = PAN, M = CVI	2D	235
	(a) AL-C; F = PAN, M = CVI	3D	215
	(b) AL-C; F = PAN, M = CVI	3D	235
	(a) Super-Carb; F = PAN, M = CVI	3D	156
	(b) Super-Carb; F = PAN, M = CVI	3D	219
BP Chemicals (Hitco) Inc.	Type CC363A; F = Pitch, M = CVI	3D	110
Carbon-Carbon Advanced Technologies, Inc.	F-23; F = Pitch, M = Resin	2D	Unknown
Carbone of America	AEROLOR A05; F = PAN, M = CVI	2D	100
Dunlop Limited / Aviation Division	ATG; F = PAN, M = CVI	2D	330
	DMS 704; F = PAN, M = CVI	2D	210
	ATA; F = PAN+Pitch, M = CVI	3D	351
Fiber Materials, Inc.	(a) 2-2-2 Fine Weave, Type A; F = Pitch, M = Pitch	3D	Unknown
	(b) 2-2-2 Fine Weave, Type A; F = Pitch, M = Pitch	3D	Unknown
	(c) 2-2-2 Fine Weave, Type A; F = Pitch, M = Pitch	3D	120
	2-2-3 Fine Weave; F = PAN, M = Pitch	3D	120
	2-2-2 Fine Weave, Type B; F = Pitch, M = Pitch	3D	220
	3D P-120; F = Pitch, M = Pitch	3D	280
	3D High Conductivity; F = Pitch, M = Pitch	3D	450
	4D Coarse Weave; F = Pitch, M = Pitch	4D	145
	4D Fine Weave; F = Pitch, M = Pitch	4D	145
Kaiser Aerotech	K-Karb 188; F = Pitch, M = Pitch	1D	550
	Type A K-Karb; F = Rayon, M = Resin+Pitch	2D	14
	K-Karb 102HS; F = PAN, M = Resin+Pitch	3D	40
Mitsubishi Chemical America, Inc.	MFC-1; F = Pitch, M = Proprietary	1D	550
	MFC-3(2); F = Pitch, M = Proprietary	3D	210
Science Applications International Corporation	SAIC 1D Rod; F = PAN, M = CVI+Pitch	1D	120
	ISOCARB 140/PAN; F = PAN, M = Resin+Pitch	4D	91
	ISOCARB 140/Pitch; F = Pitch, M = Resin+Pitch	4D	111
Sigri Great Lakes Carbon Corporation	SIGRABOND 1002 ZV 22; F = PAN, M = Resin+Pitch	2D	40
	SIGRABOND 1502 ZV 22; F = PAN, M = Resin+Pitch	2D	30
Société Européenne de Propulsion	SEPCARB N11-011; F = PAN, M = CVI	3D	220
	SEPCARB N21; F = PAN, M = CVI	3D	240
Textron Specialty Materials	Multidimensional Tile; F = Pitch, M = CVI	3D	102
	High HT Temp. Multidimensional Tile; F = Pitch, M = CVI	3D	>102
Tonen Corporation	FC-1030X; F = Pitch, M = Resin+Pitch	1D	493
Toyo Tanso USA, Inc.	CX-2002U; F = Pitch, M = CVI	2D	400
	CX-3002U; F = Pitch, M = CVI	2D	410

57 specimens tested in EBTS, 9 specimens tested in PLADIS-I

Table 2

EBTS Test Matrix For 1st Series of Electron-Beam Experiments

Case No.	Heat Flux (MW/m^2) Nominal	Heat Flux (MW/m^2) Actual	Duration (s)
1	2.5	2.5	1.5
2	5.0	5.0	1.5
3	7.5	7.5	1.5
4	15.0	15.0	1.5
5	30.0	30.0	1.5
6	45.0	45.0	1.5
7	60.0	60.0	1.5
8	75.0	75.0	1.5
9	90.0	65.0	1.5
10	105.0	92.0	1.5

Note: For each case, each specimen received one e-beam pulse. Once a specimen reached 2600°C during a specific case, it was dropped from testing in subsequent cases.

42 different CFC materials were provided by 19 CFC manufactures (Table 1).

The sample size was 2.5cm x 2.5cm x 1cm.

Multiple orientations from the same material were tested.

In the first set of EBTS tests 26 CFC samples were exposed to power densities up to 92 MW/m^2 (Table 2) for up to 1.5s. The e-beam spot size was 8 mm, and was rastered over a 100 mm^2 area (nominally 1cm x 1cm)

If the specimen temperature reached 2600^0C, the e-beam was turned off. During the first test 8 samples reached 2600^0C during the test.

In the second set of EBTS tests, 31 samples exposed to power densities up to 110 MW/m^2. Each specimen received ten 100 μs pulses. Two specimens received an additional 10 pulses (total 20 pulses) The spot size was 23mm in diameter and the energy density was 11.5 MJ/m^2; the deposited energy was 4.8kJ per pulse.

<u>EBTS test results</u>
Each specimen received up to 10, 1.5s e-beam pulses, which ranged in power from 2.5 to 92 MW/m^2. For a specimen that received all 10 full-length pulses, the deposited energy was 60 kJ.

Out of this about 10-15% of the energy goes to heating the bulk material while the remaining raises the surface temperature. No thermal shock problems (cracking) observed in any of the 26 specimens (probably because they were small in size).

Because of their low thermal conductivity, 8 of the samples could not be subjected to the highest heat fluxes (Table 2). For the remaining, the weight loss varied from 0.9 to 5.48mg. Smallest weight loss occurred in the Dunlop ATA CFC.

The thermal performance is a measure of the CFC to conduct heat in all directions simultaneously. This appears to be the reason why some CFCs with very high thermal conductivity in the through-the-thickness direction (z-direction) did not perform as well as some CFCs with lower thermal conductivity in the z-direction. The Dunlop ATA-3-D CFC (k_z of 352 W/m-K) has the highest thermal performance.

For some of the CFCs e-beam tested in multiple orientations, the level of erosion was found to be highly dependent on the how the fiber composite was aligned. This would suggest that for NSTX-U purposes, testing potential 1d, 2d or 3d CFC in multiple orientations is the only way to know how these would perform on NSTX-U. Test results for the samples are shown in the figure below.

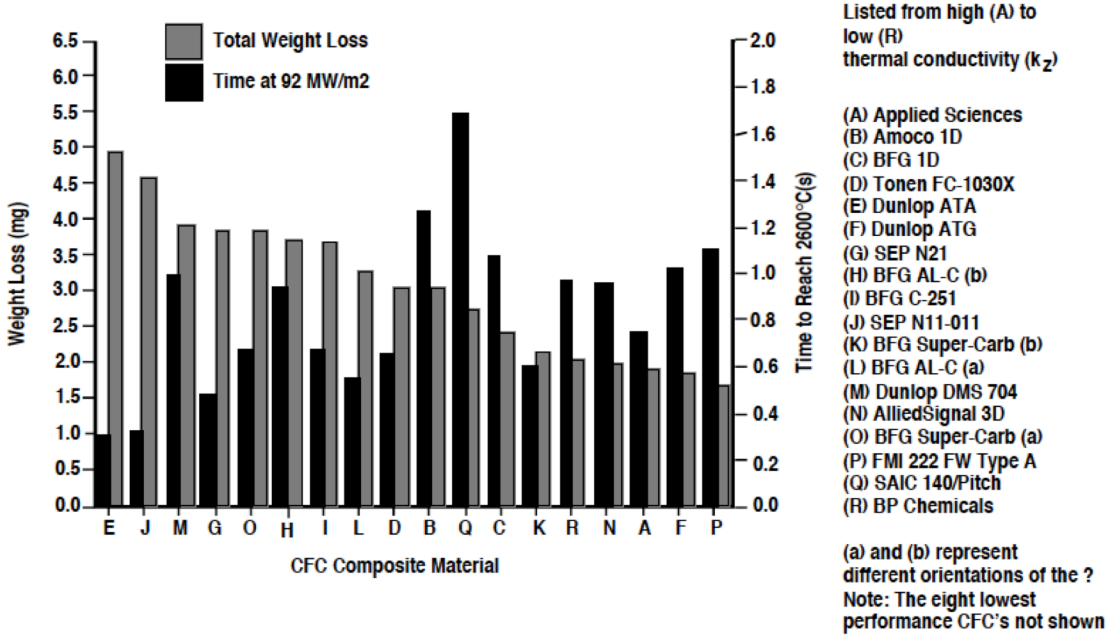

Fig. 1. EBTS e-beam test results. The total weight loss for each of the 18 CFC specimens exposed to the entire series of 10 e-beam pulses is shown. In general, the weight loss increases from left to right for the 18 CFCs, which are listed at the right in terms of high to low thermal conductivity. As a measure of the overall thermal performance of the CFCs, the time required for the specimen surfaces to reach 2600°C when exposed to a heat flux of 92 MW/m^2 is also shown. The nominal size of the e-beam heated area was 1 cm x 1 cm. The material with the best thermal performance, the Dunlop ATA 3D CFC, is shown at left. The time required to reach 2600°C decreases from left to right as the overall thermal performance decreases.

Note: The legend in the figure is incorrectly labeled. The DUNLOP 3d ATA graphite performed best. The weight loss (black bars) increases from left to right. The time to reach 2600^{0}C (grey bars) decreases from left to right. Because the Dunlop ATA is a better thermal conductor, it efficiently conducts away the heat, so the surface temperature is less, and this reduces the sublimation rate.

PLADIS-I test results

These were 100 μs plasma beam tests conducted on 9 samples. The erosion rate of 0.21 gm/MJ of absorbed energy was approximately twice that seen in the 1.5s e-beam tests. These tests have more shock loading and would increase the surface temperature at a faster rate than the e-beam tests.

The Dunlop ATA and the Mitsubishi MFC-1 performed better than the other samples. Compared to the other CFCs these had high thermal conductivity in the direction parallel to the plasma beam. As shown in the figure below there was no major differences between the samples. Two samples received a second set of 10 pulses.

HIGH HEAT FLUX TESTING OF CFC COMPOSITES
FOR THE TOKAMAK PHYSICS EXPERIMENT

P.G. Valentine, et al.

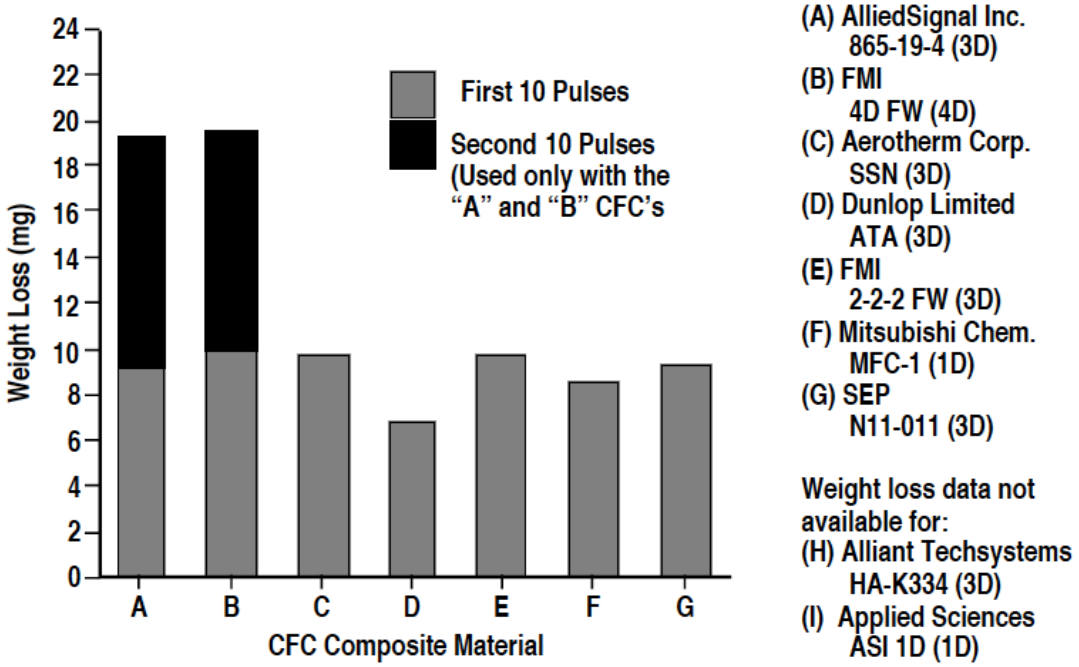

Fig. 2. PLADIS-I hydrogen plasma disruption simulation test results. The total weight loss for seven of the nine CFC specimens exposed to a series of 100-μs hydrogen plasma pulses is shown. Specimen weight loss is relatively insensitive to CFC type or thermal conductivity in the direction parallel to the plasma beam. However, there are two exceptions: the two highest conductivity materials (Dunlop ATA 3-D and Mitsubishi MFC-1 1-D) eroded at rates less than those observed with the other five CFCs shown (32% and 13%, respectively). Each plasma pulse had an energy density of 11.5 MJ/m^2; the plasma beam had a nominal diameter of 23 mm.

Sublimation tests at 2400K

Graphite sublimation tests for target development for the muon collider /neutrino factory, by C. Tsai, et al., (IEEE, 2002)[4]

Sublimation rates of graphite foils at ~2400K in a vacuum are consistent with theoretical predictions. Tests were conducted based on volumetric heat deposition (~250 MW/m^3). These are higher than the temperatures we plan to operate at and probably not of high relevance to our work. The most relevant figure is pasted below. A graphite rod 15mm in diameter and 80cm long was used for these tests (J.R. Haines, et al., presentation in 2002 & related to the paper by Tsai)

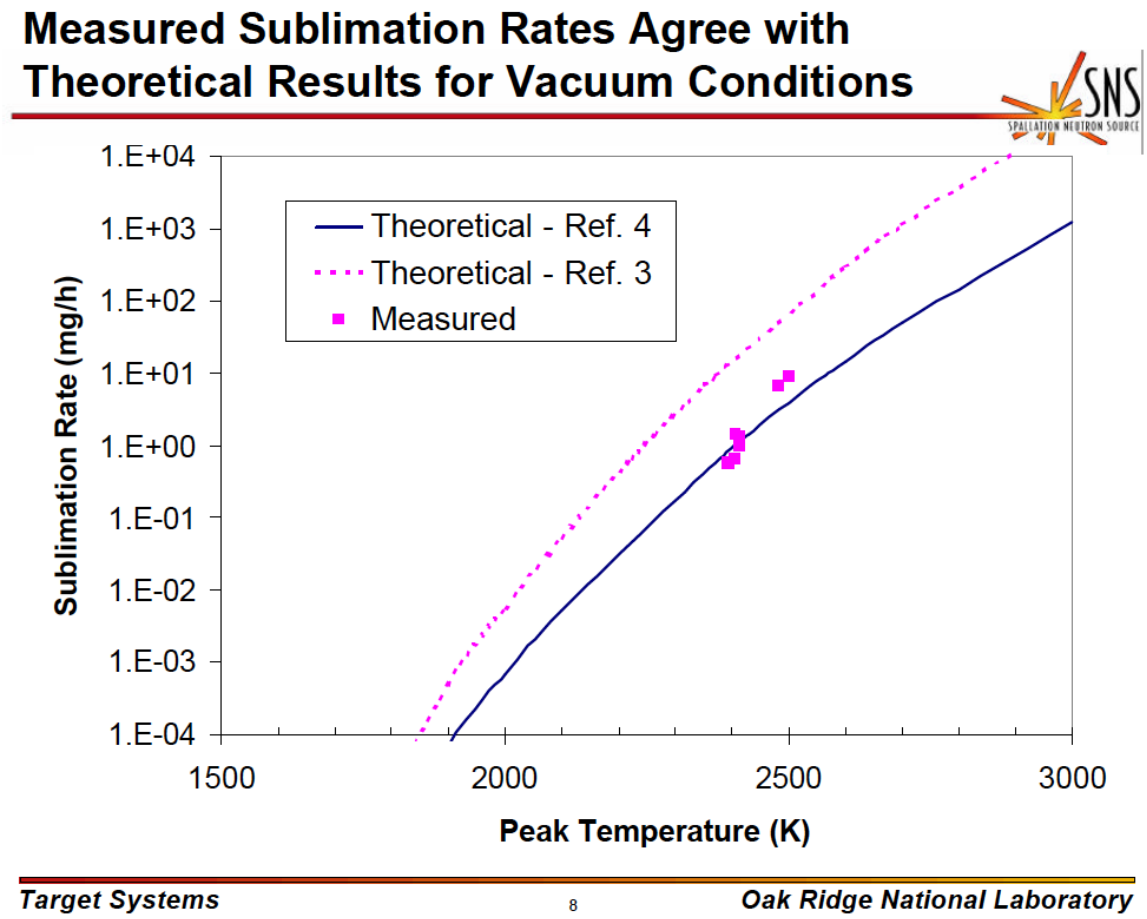

Fine grained graphite erosion at ELM-like heat loads- 20-60 MJ/m^2

Tests in the Plasma Trap GOL-3 (mirror machine type set-up), by A.V. Burdakov, et al., European congress on advanced materials, Prague (2005)[5]

Fine grained, high-density graphite tested by the Budker institute in Russia.

The erosion depth depends on the energy density and reaches 0.5 to 1 mm at 20-60 MJ/m^2 in short pulse tests (10 micro seconds, hot plasma electrons ~2keV). The most relevant figure (for our purposes) is pasted below.

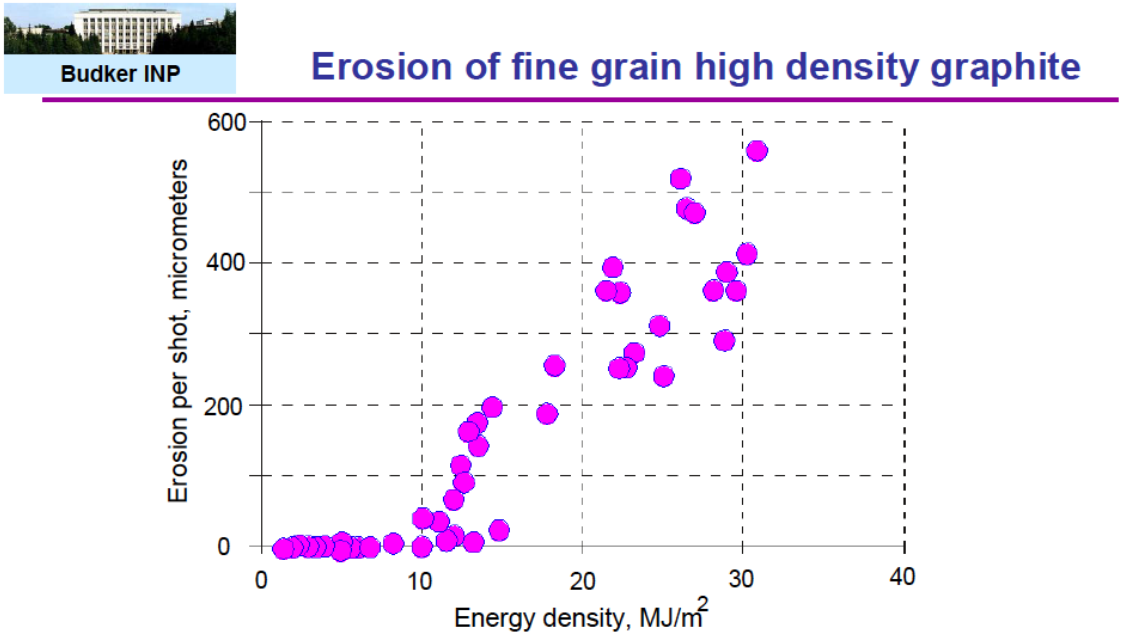

Irradiation of the graphite target by a stream of the plasma hot electrons together with the relativistic electron beam leads to explosive (brittle) erosion of the graphite. The erosion depth of the graphite depends on the energy density and reaches 0.5-1 mm at 20-60 MJ/m^2.

Recommendations

1. Experimental tests conducted in support of selecting graphite based CFCs for ITER suggest that suitable graphite materials may be able to exceed the 1600^0C temperature limit for PFCs that is currently being adopted for NSTX-U. So, this is a conservative value to use at this time, and it can later be upgraded to a higher temperature based on experimental tests noted below.

2. Results also show that if the CFC material is properly oriented (within ±15 degree tilt to the preferred axis for maximizing heat conduction), both the surface temperature and erosion could be well controlled.

3. CFCs can outperform fine grained graphite both in limiting the surface temperature and maintaining strength.

4. It is recommended that the NSTX-U engineering team obtain samples of the following materials and test them in a heat flux test facility, and based on these tests select the material of choice for NSTX-U.
    1) Fine grained graphite: Sigrafine R6510 & or IG-43 from Toyo Tanso
    2) Felt type CFC: CX2002U (from Toyo Tanso)
    3) 3D-CFC: NB31 or 41[6]
    4) 2D-CFC: One or two more such as the DUNLOP DMS704 (TD02 material chosen by JET) or DMS780

    This is because; there are a number of CFCs that may perform well on NSTX-U, as long as they are properly oriented with respect to the field lines striking the tiles. The studies conducted as part of the tests for ITER indicate that alignment inaccuracies of ±15% may be acceptable. So, an actual test of each of these materials would be the best way to select the material of choice for NSTX-U.

    It is also recommended that one member from the engineering team and one member from the physics team be assigned to travel to a suitable test site to conduct these tests ASAP.

    Which of the above referenced materials are used would depend of which ones are available on a reasonable time, and how much they cost. So, it may not be possible to test all of the above referenced materials.

    Prior to the test, the orientation that would be used for these materials on NSTX-U should be identified so that the tests could be conducted under this specific orientation. Based on the reported test results, we know they will perform well if perfectly aligned, so the tests for NSTX-U should be conducted under realistic fiber alignment conditions.

5. These tests would not only allow the best available material to be chosen for NSTX-U applications, but may also allow the maximum temperature limits to be increased to above 1600C.

6. If the graphite tiles are physically small in size, the mechanical strength is probably not an issue. So materials with good thermal conduction, and not so good structural strength, may be acceptable for NSTX-U applications.

   If larger graphite tiles are used in NSTX-U, then the above experimental tests need to be used in conjunction with more effort on modeling these large tiles, to establish the operating limits for these larger tiles.

7. Because it may take at least a year or more for NSTX-U to reach full-power operations, as it will take time to test the numerous systems and diagnostics, the project should consider using the existing graphite tiles, and implementing the new graphite tile upgrade during an outage approximately 1 to 1.5 years after restart of NSTX-U operations.

   During this 1 – 1.5 Yr period the discharges that are run on NSTX-U could be better identified to avoid field line strikes intersecting the PF1C casing (as was done for the 2016 run campaign)

8. The initial long-pulse, high power, operations on NSTX-U should use a simple radiative divertor configuration, to reduce heat load to the tiles. In controlled experiments, the divertor gas-puffing amount should be reduced and the corresponding increases to the tile temperature (and the localization) should be measured to further quantify the tile capability on NSTX-U to support 5s, high-power operations.

References

[1] M. Ulrickson, Jour. Nuclear Materials 176 & 177 (1990) 44-50
[2] M.A. Pick, et al., Jour. Nucl. Materials 220-222 (1995) 595
[3] P.G. Valentine, et al., GA-A22206 (February, 1996), https://fusion.gat.com/pubs-ext/ICFRM95/A22206.pdf
[4] Graphite sublimation tests for target development for the muon collider /neutrino factory, by C. Tsai, et al., (IEEE, 2002)

[5] A.V. Burdakov, et al., European congress on advanced materials, Prague (2005)
[6] Analysis of carbon based materials under fusion relevant thermal loads.

Analysis of Carbon Based Materials under Fusion Relevant Thermal Loads

Von der Fakultät für Maschinenwesen der Rheinisch-Westfälischen
Technischen Hochschule Aachen
zur Erlangung des akademischen Grades eines Doktors
der Naturwissenschaften genehmigte Dissertation

vorgelegt von

Jérémie Saint-Hélène COMPAN
aus
Paris, Frankreich

Berichter: Univ. Prof. Dr.-Ing. Lorenz Singheiser
Univ. Prof. Dr.-Ing. Tilmann Beck

Tag der mündlichen Prüfung: 17.09.2008

Diese Dissertation ist auf den Internetseiten der Hochschulbibliothek online verfügbar